Applied Catalysis B: Environmental 100 (2010) 481–490

Contents lists available at ScienceDirect

Applied Catalysis B: Environmental

journal homepage: www.elsevier.com/locate/apcatb

Catalytic hydrogen combustion for treatment of combustible gases from fuel cell processors

Parag A. Deshpande, Giridhar Madras*

Department of Chemical Engineering, Indian Institute of Science, Bangalore 560012, India

ARTICLE INFO

Article history:
Received 12 May 2010
Received in revised form 26 August 2010
Accepted 28 August 2010
Available online 23 September 2010

Keywords:
Catalytic combustion
Combustion synthesis
Ionic catalysts
Redox couples
XPS
Dual site mechanism

ABSTRACT

Catalytic combustion of H_2 was carried out over combustion synthesized noble metal (Pd or Pt) ion-substituted CeO_2 based catalysts using a feed stream that simulated exhaust gases from a fuel cell processor. The catalysts showed a high activity for H_2-combustion and complete conversion was achieved below 200 °C over all the catalysts when O_2 was used in a stoichiometric amount. With higher amounts of O_2, the reaction rates increased and complete conversions were possible below 100 °C. The reaction was also carried out over Pd-impregnated CeO_2. The conversions of H_2 with stoichiometric amount of O_2 were found to be higher over Pd-substituted compound. The mechanism of the reaction over noble metal-substituted compounds was proposed on the basis of X-ray photoelectron spectroscopy studies. The redox couples between Ce and metal ions were established and a dual site redox mechanism was proposed for the reaction.

1. Introduction

Fuel cell technology for energy systems is attractive both from energy as well as environmental viewpoints. Due to the direct conversion of the chemical energy to electrical energy, the efficiency of such systems is not limited by the Carnot efficiency [1]. The performance of the conventional thermal heat engine systems becomes inferior compared to that of a fuel cell system due to highly irreversible nature of the combustion reaction [2]. The products of the reaction from a fuel cell processor are cleaner as compared to those from thermal engine systems, which inherently produce hazardous gases like CO and NO_x. Fuel cell processors have a wide range of potential applications including those in automobile and propulsion systems, domestic and industrial supply [3], and such systems are also seen as systems for cogeneration of heat and electricity [4].

Fuel cells utilizing H_2 have several advantages like high energy density, low operating temperature and fast response to load changes [5]. However, the use of H_2 poses a potential environmental hazard because all H_2 supplied to the fuel cell is not consumed. In some cases, excess H_2 has to be supplied to maintain a stable voltage [6], which results in a higher amount of unreacted H_2 in the system. One of the strategies to overcome this problem is the recycling of the exhaust gases from the fuel cell processor. However, this increases the complexity of the system and recycling becomes practical only for large systems [7]. Even in the case of systems with recycle, the exhaust gas cannot be made completely free from H_2 and some residual H_2 is always observed in the outlet stream. Accumulation of H_2 can result in the formation of combustible or explosive mixtures. Such accidents have indeed been observed in the past [8]. Therefore, it is very important process the exhaust gases for the removal of residual H_2.

The combustion of H_2 is a highly exothermic reaction with an enthalpy of reaction of −286 kJ/mol. Therefore, the reaction is accompanied by a large increase in temperature. H_2 has a wide flammability range of 4–75% [9]. Direct flame combustion of H_2 has been investigated by several investigators [10–12]. However, catalytic combustion offers several advantages over flame combustion. According to Vlachos and co-workers [13–15], homogeneous flame combustion is the preferred mode of combustion of hydrocarbons only for large scale operations and with reduction in system volume, the coated wall reactors show better and more stable performance. Due to the highly exothermic nature of the reaction, it is desirable to carry out the reaction in microcombustors. Kaisare et al. [16,17] have studied the catalytic combustion in wall coated microcombustors. Structured monolithic reactors have also been used to study the catalytic combustion of H_2 and hydrocarbons [18].

As pointed out by Ladacki et al. [19], in spite of the importance of H_2–O_2 reaction for energy and environmental applications, this reaction has not been well explored. Whereas the catalytic combustion of CH_4 has been widely studied over different noble metals and different supports [20–24], there have been a few reports of

* Corresponding author. Tel.: +91 80 2293 2321; fax: +91 80 2360 0683.
E-mail addresses: giridhar@chemeng.iisc.ernet.in, giridharmadras@gmail.com (G. Madras).

0926-3373/$ – see front matter © 2010 Elsevier B.V. All rights reserved.
doi:10.1016/j.apcatb.2010.08.026

H_2–O_2 combination over a number of metals including Ni, Cu, Pd, Ag and Au [25–29] and over supported catalysts like Al_2O_3 and Fe_2O_3 [26,30]. In this study, we have carried out the catalytic combustion of H_2 in a H_2-lean gas mixture that simulated typical fuel cell processor conditions. We have synthesized a series of Pd and Pt ion-substituted CeO_2 compounds and the related solid solutions. We have previously reported high catalytic activity of these compounds for CO oxidation and NO_x reduction [31,32]. We have tested the activity of the catalysts for catalytic H_2-combustion. The use of a reducible support is expected to enhance rate of reaction by the involvement of the lattice oxygen.

2. Experimental

2.1. Catalyst synthesis

Noble metal (Pd and Pt) ion-substituted CeO_2 solid solutions were prepared using the solution combustion technique. Three different modifications of the support were used. Apart from pure CeO_2, 15% Zr and Ti ions were substituted in the support CeO_2 to obtain $Ce_{0.85}Zr_{0.15}O_2$ and $Ce_{0.85}Ti_{0.15}O_2$, respectively. 2 at.% substitution of the noble metal was carried out. Therefore, the compounds synthesized were $Ce_{0.98}Pd_{0.02}O_{2-\delta}$, $Ce_{0.98}Pt_{0.02}O_{2-\delta}$, $Ce_{0.83}Zr_{0.15}Pd_{0.02}O_{2-\delta}$, $Ce_{0.83}Zr_{0.15}Pt_{0.02}O_{2-\delta}$, $Ce_{0.83}Ti_{0.15}Pd_{0.02}O_{2-\delta}$ and $Ce_{0.83}Ti_{0.15}Pt_{0.02}O_{2-\delta}$, where δ represents the oxide ion vacancy created due to substitution of the metal in ionic form. For the synthesis of the compounds, the precursor nitrates of all the elements were dissolved in a solution in a stoichiometry given by the chemical formula and a fuel (glycine) was added. The amount of glycine required was calculated by making a balance over the oxidizing and the reducing valences in the solution [33]. The solution was made to undergo combustion in a furnace at 350 °C. Further details on the synthesis of the compounds can be found elsewhere [31,33]. Pd-impregnated CeO_2 was also prepared using wet impregnation technique for comparing the activity of metal ion-substituted catalysts. 2 at.% substitution of Pd in CeO_2 corresponds to 1.25 wt% of Pd in Pd-impregnated CeO_2 and, therefore, 1.25 wt% Pd/CeO_2 was synthesized. CeO_2 was synthesized by the solution combustion technique. A slurry of CeO_2 and $PdCl_2$ was made and a dilute solution of hydrazine hydrate in water was added slowly to the slurry to reduce Pd salt to Pd nanoparticles, which got deposited over support CeO_2. The solids were filtered and washed with ethanol and solicited for 15 min. The wet solids obtained were heated at 150 °C for 4 h to obtained Pd-impregnated catalyst.

2.2. Catalyst characterization

The compounds were characterized by powder X-ray diffraction (XRD) and X-ray photoelectron spectroscopy (XPS). XRD patterns of all the compounds were recorded on a Phillips X'pert diffractometer in 2θ range of 20–90° with a step size of 0.067°. The XPS of all the elements in the compounds were recoded on Thermo Fisher Multilab ESCA with AlKα radiations of energy 1486.6 eV. All the peaks were calibrated with respect to graphitic of C1 s peak with a binding energy of 284.5 eV and confirmed with the binding energy of O1s.

2.3. Catalytic reactions

The gas phase catalytic combustion reactions were carried out in glass tube reactors of 9 mm I.D. The catalyst granules of size 300–600 μm size were diluted with silica granules of the same size. Due to highly exothermic nature of the reaction, the catalyst weight was minimal (10 mg) and diluted with silica to make a total bed weight of 1 g and bed length of 1.5 cm. Uniform dispersion of the catalyst particles in the diluent was ensured for each catalyst bed. The catalyst bed was made between two plugs of ceramic wool. A thermocouple was placed in the catalyst bed to measure the temperature of the bed. The reactor was heated from outside by an electric heater and the temperature was controlled using a PID temperature controller. The reactions were carried out under isothermal conditions. Due to exothermicity of the reaction, a gradual increase in the bed temperature was indeed observed but the increase of the temperature was very small such that the reaction can be considered to be taking place essentially under isothermal conditions. The reactant gas mixture consisted of H_2, O_2 and N_2 (Shri Vinayaka Gases, Bangalore, India). In all the reactions, a total flow rate of 200 ml/min was maintained. The concentration of H_2 was fixed at 2.75 mol%. The amount of O_2 in the mixture was varied. Reactions with 1.38 mol% and 2.75 mol% of O_2 were carried out, which corresponded to the O_2 stoichiometry of 1 and 2, respectively, required for the combustion reaction. The gases were sent through control valves to obtain the required composition. The reactions were also carried out using simulated air conditions in which the amount of O_2 in the reactant gas corresponded to the composition of air. Typically, the reaction mixture had a composition of H_2:O_2:N_2 = 5.5:41.5:153. The reactions were also carried out in the presence of CO to observe the effect and co-oxidation of CO. For the reactions in the presence of CO, 2.75 mol% H_2, 2.75 mol% CO and 2.75 mol% O_2, balanced with N_2, were used. The composition of the products and the unreacted gas mixture was determined using an online gas-chromatograph (Mayura Analyticals, Bangalore, India) using a combination of Hayesep – A and molecular sieve columns. The detection was accomplished by a thermal conductivity detector and a flame ionization detector.

3. Results and discussion

3.1. Catalyst characterization

The crystal structure of the catalysts was established using XRD. Fig. 1 shows the XRD of unsubstituted and noble metal ion-substituted catalysts. Fig. 1(a) shows the XRD of CeO_2, $Ce_{0.98}Pd_{0.02}O_{2-\delta}$ and $Ce_{0.98}Pt_{0.02}O_{2-\delta}$. The lines in the XRD of CeO_2 correspond to the cubic structure with a space group of F*m3m*. On comparing the XRD of metal ion-substituted CeO_2 with unsubstituted CeO_2, it can be seen that all the compounds have the same structure and the metal ions were substituted in the lattice. However, this exclusively may not show the substitution of the ions in the lattice. A very fine dispersion of Pd/Pt nanoparticles in CeO_2 matrix may not result in any appreciable peak in the XRD pattern. However, the substitution of the metals in the lattice results in the changes in the lattice parameters owing to the differences in the ionic radii of Ce^{4+} and M^{2+} (M = Pd/Pt). Therefore, Rietveld refinement of the patterns was carried out. It was found that changes in the lattice parameter occurred on substitution [34]. Further, we have previously established the structure of the compounds using several techniques including XRD, FT-Raman, TEM, and EXAFS and have found that the metal ions were indeed substituted in the lattice and were not present as oxides (PdO or PtO) and also not as a fine dispersion of metal [31].

Bulk substitution of Zr^{4+} and Ti^{4+} ions in Ce^{4+} sites was carried out with 15 at.% substitution. The XRD of $Ce_{0.85}Zr_{0.15}O_2$ and $Ce_{0.85}Ti_{0.15}O_2$ are shown in Fig. 1(b) and (c), respectively, and the patterns match with the cubic structure. Therefore, the parent CeO_2 structure was retained on bulk substitution and the compounds were indeed solid solutions. The Rietveld refinement of $Ce_{0.85}Zr_{0.15}O_2$-based compounds showed the difference in the lattice parameter compared to that of the parent compound showing the substitution of the compounds [34]. The superior values of the

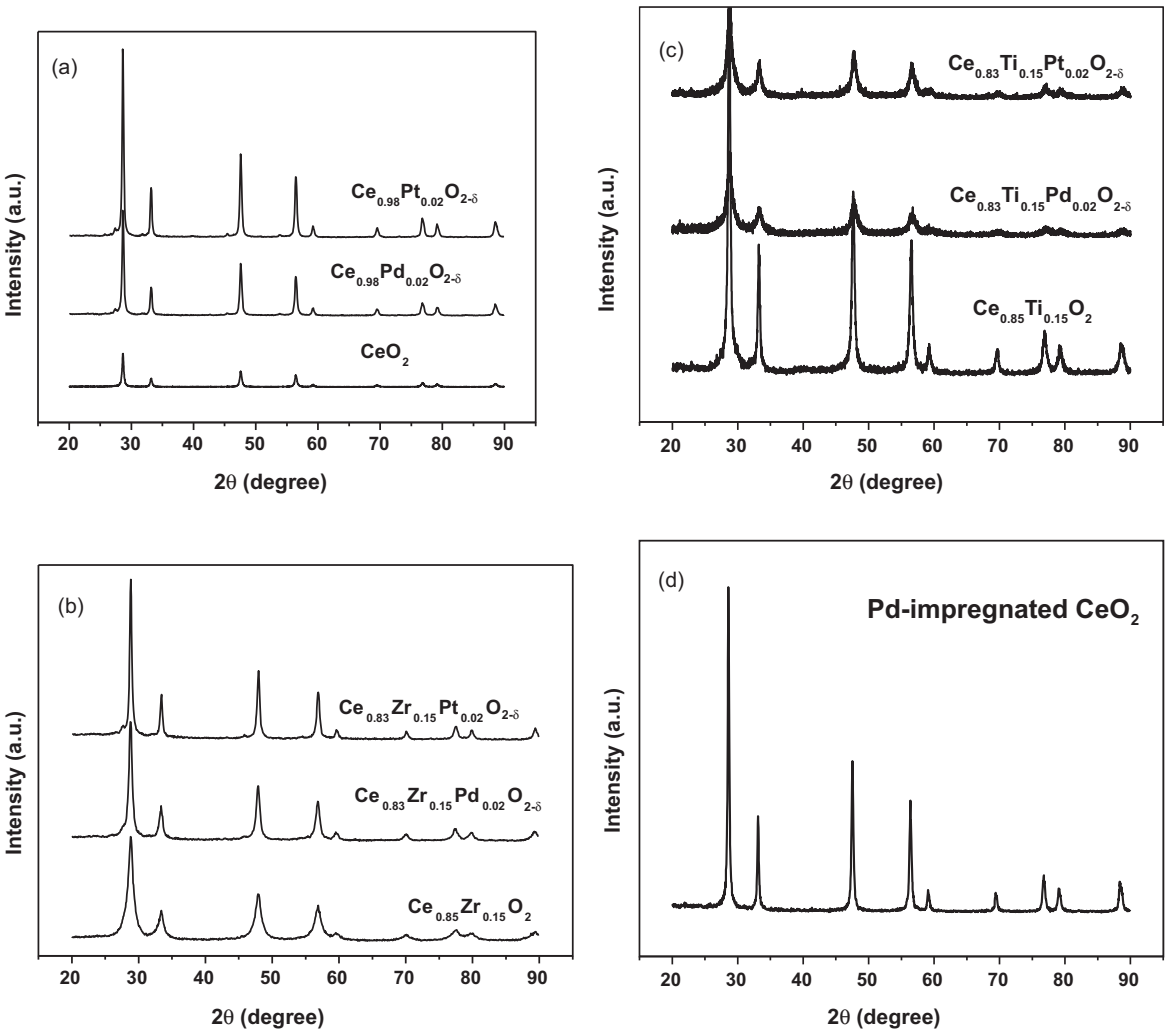

Fig. 1. XRD of (a) CeO_2 and Pd/Pt-substituted CeO_2, (b) $Ce_{0.85}Zr_{0.15}O_2$ and Pd/Pt-substituted $Ce_{0.85}Zr_{0.15}O_2$, (c) $Ce_{0.85}Ti_{0.15}O_2$ and Pd/Pt-substituted $Ce_{0.85}Ti_{0.15}O_2$, (d) 1.25 wt% Pd-impregnated CeO_2.

reliability parameters for homogeneous solid solution compared to separate phases further confirm the formation of solid solutions. Further, FT-Raman studies have shown the crystallization of the compound in single phase cubic structure and no tetragonal phase separation corresponding to ZrO_2 was observed in case of $Ce_{0.85}Zr_{0.15}O_2$ [34]. Therefore, all the catalysts synthesized in this study had cubic fluorite structure with metal ions substituted in the lattice, occupying the Ce^{4+} sites. Kaspar and co-workers have extensively explored the effect of composition and dopants in CeO_2–ZrO_2 systems [35–38]. CeO_2–ZrO_2 mixed systems have been explored along with trivalent metal doping. It was observed that on doping, the homogeneity of cubic phase in $Ce_{0.6}Zr_04O_2$ was enhanced. The solid solutions were also found to show improved oxygen exchange [35]. The thermal stability of the compounds is enhanced on thermal treatment and phase separation does not take place and these systems bear advantages of tunable redox properties and ability to provide highly ordered systems [39]. In this study, we have also obtained single phase compounds with no impurities. The single phase system was observed to be retained and on thermal treatment also, no phase separation took place, as signified by the XRD and Rietveld refinement of the treated compounds.

To compare the activity of ionically substituted Pd/Pt CeO_2 synthesized by the solution combustion technique with the activity of Pd/Pt CeO_2 catalysts synthesized by conventional impregnation techniques, Pd-impregnated CeO_2 was also synthesized. Fig. 1(d) shows the XRD of Pd-impregnated CeO_2. It can be seen that no appreciable peak corresponding to Pd metal is observed in this case. As mentioned earlier, a fine dispersion of the metal in the matrix can result in non-detection of the metal peak. The amount of Pd in the catalyst was only 1.25 wt% and this is very small for the proper detection by XRD. However, very weak Pd peaks have been observed by Baidya et al. [39] for 2% substitution. The absence of metal peak shows the achievement of very fine dispersion of Pd nanoparticles in CeO_2. Dispersion of the nanoparticles is important as the catalytic activity depends upon the extent of dispersion in the support matrix.

A detailed characterization of the electronic structure of the compounds was carried out using XPS. The observations from XPS are discussed later in relation with the mechanism of the reaction taking place over the catalysts.

3.2. Catalytic hydrogen combustion over the catalysts

Combustion of H_2 was carried out over noble metal-substituted compounds. The variation of H_2 conversion with temperature is shown in Fig. 2(a)–(f). With stoichiometric amount of O_2 in the feed (H_2:O_2 = 2:1), 95% and above conversion of H_2 over the various catalysts took place within 200 °C. $Ce_{0.98}Pd_{0.02}O_{2-\delta}$ showed relatively lower activity as compared to the other catalysts. The initial activity of the catalyst was low and only 10% conversion

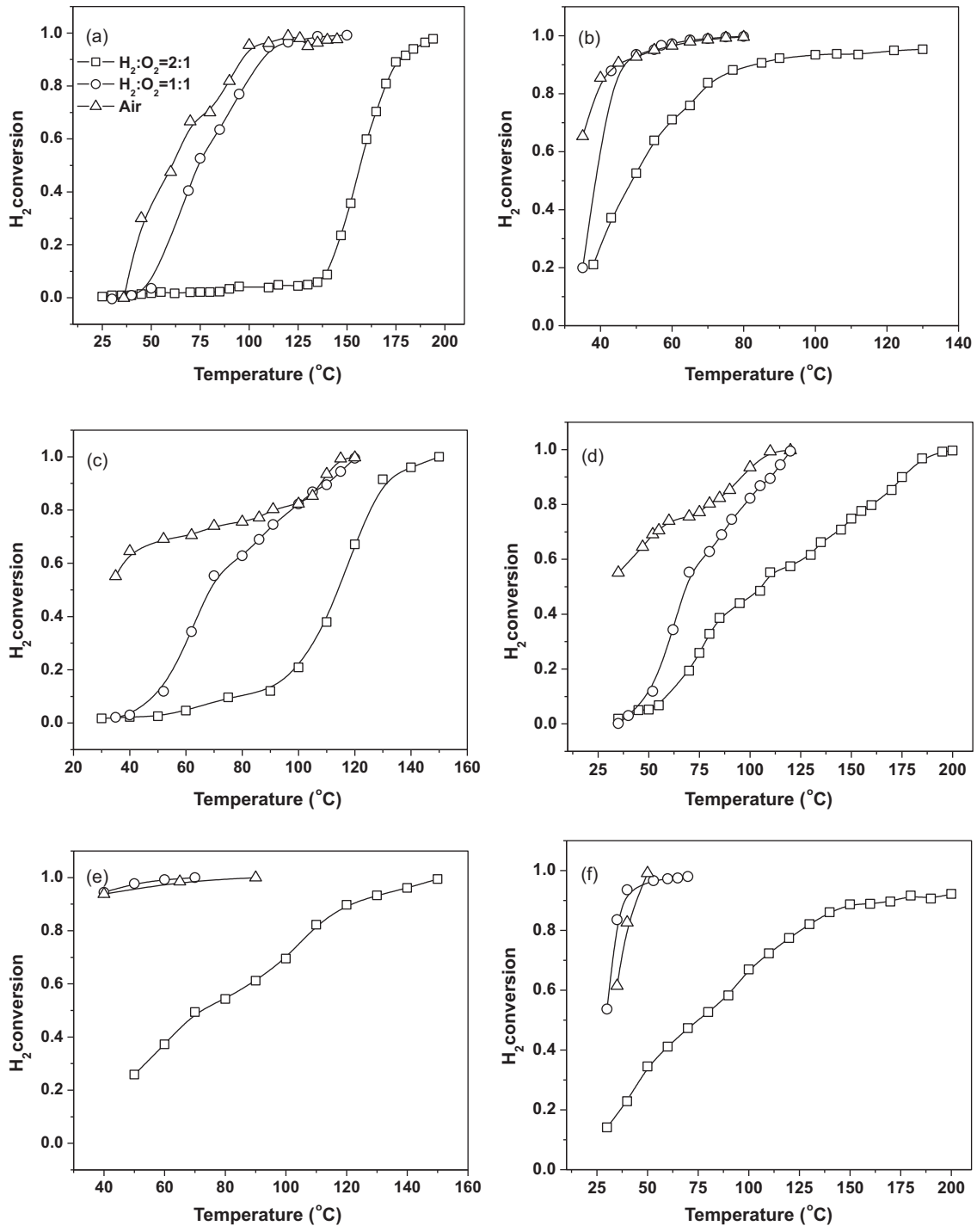

Fig. 2. Variation of H_2 conversion with temperature for H_2-combustion over (a) $Ce_{0.98}Pd_{0.02}O_{2-\delta}$, (b) $Ce_{0.98}Pt_{0.02}O_{2-\delta}$, (c) $Ce_{0.83}Zr_{0.15}Pd_{0.02}O_{2-\delta}$, (d) $Ce_{0.83}Zr_{0.15}Pt_{0.02}O_{2-\delta}$, (e) $Ce_{0.83}Ti_{0.15}Pd_{0.02}O_{2-\delta}$ and (f) $Ce_{0.83}Ti_{0.15}Pt_{0.02}O_{2-\delta}$.

could be obtained at 150 °C (Fig. 2(a)). However, a sharp light off was observed subsequently and more than 90% conversion was observed within 180 °C. The concentration of H_2 in the product was negligible above 200 °C. The conversions over $Ce_{0.98}Pt_{0.02}O_{2-\delta}$ were found to be high; more than 80% conversion was possible below 80 °C (Fig. 2(b)). The conversions did not increase subsequently and nearly 95% conversion was possible at 140 °C. In case of Pd-substituted CeO_2, an exponential increase in conversion was observed at lower conversions, Pt-substituted CeO_2 showed very high conversions even at low temperatures and a light off was observed at 40 °C itself. The conversions over Pd ions, substituted in $Ce_{0.85}Zr_{0.15}O_2$ and $Ce_{0.85}Ti_{0.15}O_2$ were found to be higher than that over $Ce_{0.98}Pd_{0.02}O_{2-\delta}$. Complete conversions within 150 °C were possible (Fig. 2(c) and (e)). Trovarelli and co-workers have established the role of alkali, transition and rare earth metals on CeO_2 based catalysts for combustion reactions [40–43]. The effect of bulk substitution of Zr and Ti on the reducibility of the support, and hence the rates of reaction has been reported for combustion synthesized compounds [39,44]. CO oxidation reaction has been found to be higher over $Ce_{0.85}Zr_{0.15}O_2$ and $Ce_{0.85}Ti_{0.15}O_2$ compared to that over CeO_2. The formation of differential bond lengths and enhancement in the reducibility on bulk substitution were attributed to

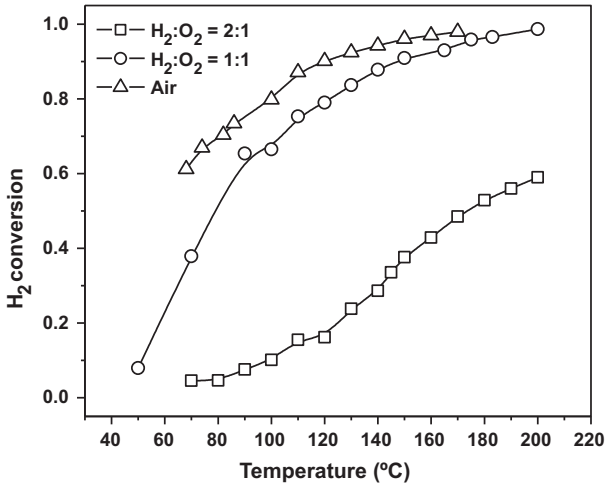

Fig. 3. Variation of H_2 conversion with temperature for H_2-combustion over Pd-impregnated CeO_2.

an increase in the activity of the compounds. In the present study also, we have found a similar trend for H_2-combustion reaction. Therefore, the involvement of the support in the reaction can be expected during the reaction. The implications of the support identity, reducibility and metal-support interactions on the reaction mechanism are discussed subsequently. The effect of bulk substitution on Pt ion-substituted catalysts was less pronounced as compared to that in the case of Pd ion-substituted compounds (Fig. 2(d) and (f)). This is probably because the dissociation of H_2 over Pt ions is higher as compared to that over Pd ions. Therefore, with $Ce_{0.98}Pt_{0.02}O_{2-\delta}$ itself, the conversions obtained were very high and further increase in the reducibility did not have a substantial effect on the activity of the catalyst.

The reactions were carried out with higher amounts of O_2 in the feed. In one set of reactions, O_2 used was twice that required by the reaction stoichiometry (H_2:O_2 = 1:1) while in the other, O_2 in the feed corresponded to that in air (H_2:O_2 = 1:7.5). It was found that a large increase in the rate of reaction occurs with an increase in the supply of O_2. When O_2 was twice the stiochiometric requirement (H_2:O_2 = 1:1), 95% conversion was achieved below 100 °C over all the catalysts. A large increase in the conversions was observed on increasing the amount, as observed in Fig. 2(a). Though only 10% conversion was possible at 150 °C with stoichiometric amount of O_2, 95% conversion was achieved at the same temperature when O_2 was twice the stoichiometric requirement. Similarly a large decrease in temperature requirement was observed for other Pd-substituted supports (Fig. 2(c) and (e)). Nearly 90% conversion was observed over $Ce_{0.83}Ti_{0.15}Pd_{0.02}O_{2-\delta}$ at 40 °C. Pt-substituted compounds also showed a high increase in conversions with more than 50% conversion at 30 °C. When the reaction was carried out with O_2 in the feed corresponding to that in air (H_2:O_2 = 1:7.5), the conversions were found to increase further (Fig. 2(a)). Negligible conversions were observed over $Ce_{0.98}Pd_{0.02}O_{2-\delta}$ at 50 °C with H_2:O_2 = 2:1 and 1:1, nearly 40% conversion was observed with H_2:O_2 = 1:7.5. Similarly, the conversions were higher at lower temperatures over $Ce_{0.98}Pt_{0.02}O_{2-\delta}$ (Fig. 2(b)). However, at higher temperatures, nearly the same conversions were observed with both H_2:O_2 = 1:1 and 1:7.5. $Ce_{0.83}Ti_{0.15}Pd_{0.02}O_{2-\delta}$ and $Ce_{0.83}Ti_{0.15}Pt_{0.02}O_{2-\delta}$ showed very high activity with nearly 90% conversions observed at 40 °C.

Fig. 3 shows the variation of H_2 conversion with temperature over Pd-impregnated catalysts. Complete conversions were observed over both impregnated as well as substituted compounds below 200 °C. The activity of Pd-impregnated compound was slightly higher up to 150 °C with stoichiometric O_2 (H_2:O_2 = 2:1). While 10% conversion was observed over Pd-substituted CeO_2, nearly 20% conversion was observed over Pd-impregnated CeO_2. However, at higher temperatures, a large difference in the activity of the compounds was observed. 95% conversion was observed over Pd-substituted CeO_2 at 200 °C while only 60% conversion was observed over Pd-impregnated CeO_2 at the same temperature. Therefore, Pd ion-substituted catalysts showed superior activity over Pd-impregnated catalyst, signified by a large difference in the conversions observed over the two catalysts at 200 °C.

The presence of CO in the feed can pose severe problems of catalyst poisoning. CO adsorbs preferentially over noble metals and, therefore, the activity of the catalyst towards the oxidation of H_2 may be affected. There have been studies on the adsorption of both CO as well as H_2 over noble metals and it was found that adsorption of CO was higher as compared to the adsorption of H_2 [45–47]. Therefore, it is important to study the effect of the presence of CO in the feed. The activity of the catalysts was tested with an equal amount of CO in the feed. Fig. 4 shows the conversions of H_2 and CO obtained in the presence of CO. It can be observed that the temperature requirement for a given conversion increased. However, for all the catalysts, complete conversion of H_2 was possible within 250 °C. This shows that the catalyst remains active even in the presence of CO. Nearly complete conversion of CO to CO_2 was possible within 300 °C over all the catalysts. The effluents can be treated without further heating as the operating temperature of a fuel cell is close to the working temperature of the catalysts.

The surface areas of all the compounds were in the range of 20–25 m^2/g. For ionically substituted systems, the role of surface area is secondary and if there is no significant difference in the surface areas of the catalysts, the variation in the activities of the catalyst can be attributed to the differences in the electronic interactions taking place in the system. Therefore, we carry out the analysis for the kinetics of the reaction on the basis of the redox couples set in the catalyst. The analysis in the current study is based upon the light off temperature and the variation of conversions with temperature. Further investigations might be required for describing the kinetics of the reactions. However, CHC being a highly exothermic reaction, the current set of conditions were chosen after several experiments so as to obtain the optimal conditions for proper kinetic description of the reaction. An increase in either the weight of the catalyst or a decrease in the space velocity resulted in a high temperature rise in the systems. Therefore, the current analysis with the reported set of conditions presents a correct qualitative description of the reaction.

3.3. Mechanistic insights using spectroscopy

As mentioned earlier, the effect of support on the reaction rates indicates the involvement of support in the surface processes taking place over the catalyst. To obtain an insight into the mechanism of H_2-combustion over the synthesized catalysts, we trace the changes in the electronic structure of the compounds by XPS before and after the reaction. The metal-support interactions established using XPS was used to propose a probable mechanism for the reaction.

Fig. 5 shows the XPS of Ce3d in the various catalysts before and after reaction. It can be seen that in all the compounds, Ce was present in 4+ state except in $Ce_{0.83}Ti_{0.15}Pd_{0.02}O_{2-\delta}$ in which small amount of Ce^{3+} can also be observed. However, after the reaction, Ce^{3+} ions emerge in the compound. This can be observed in the spectra of all Pd ion-substituted compounds. The spectra of $Ce_{0.83}Ti_{0.15}Pt_{0.02}O_{2-\delta}$ also show the same. This clearly shows the involvement of Ce^{4+}–Ce^{3+}–Ce^{4+} redox processes during the reaction. Reduction of Ce^{4+} to Ce^{3+} during oxidation reactions like CO oxidation is known [48,49]. Therefore, during the reaction it is

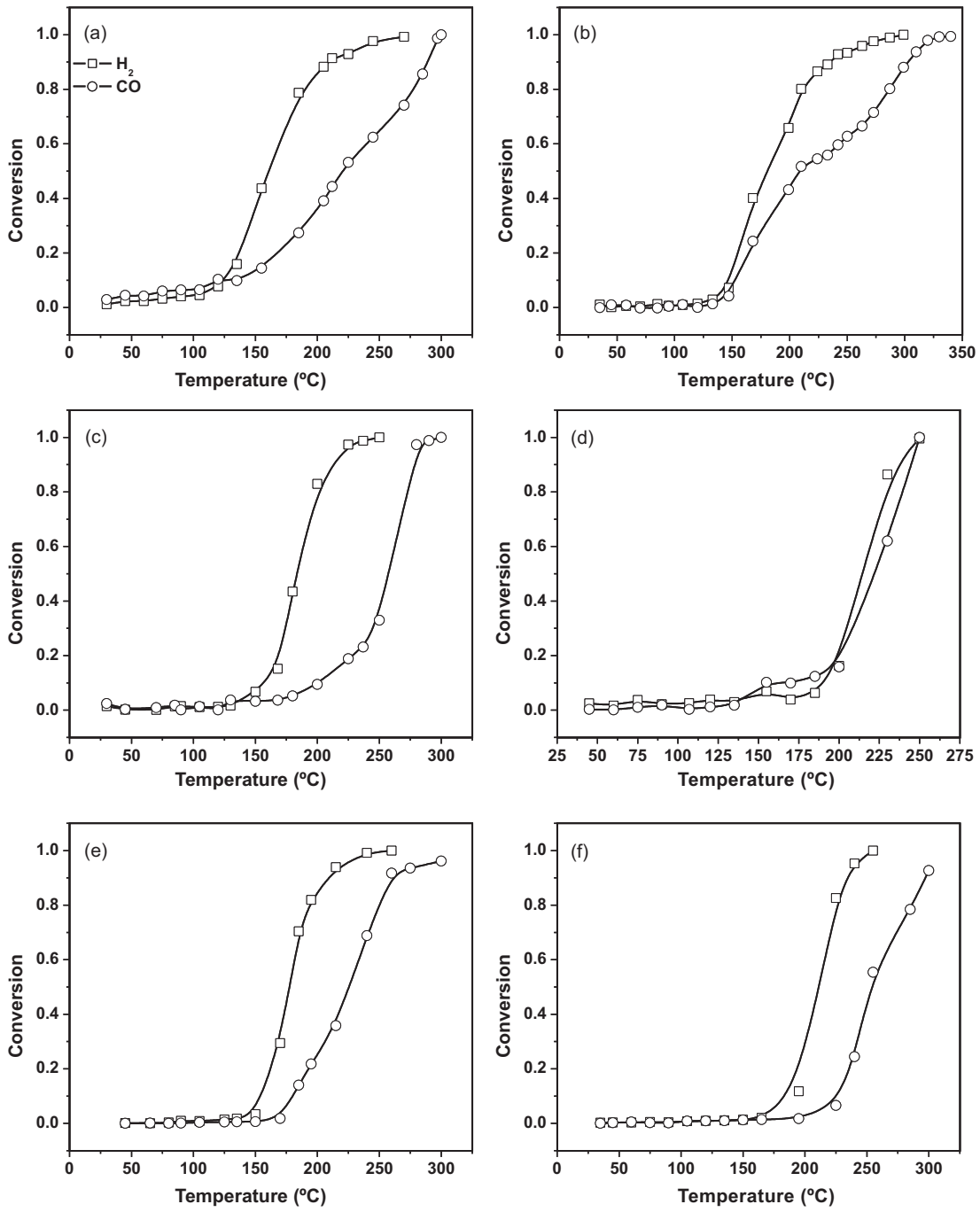

Fig. 4. Variation of H_2 and CO conversion with temperature for H_2-combustion with CO in feed over (a) $Ce_{0.98}Pd_{0.02}O_{2-\delta}$, (b) $Ce_{0.98}Pt_{0.02}O_{2-\delta}$, (c) $Ce_{0.83}Zr_{0.15}Pd_{0.02}O_{2-\delta}$, (d) $Ce_{0.83}Zr_{0.15}Pt_{0.02}O_{2-\delta}$, (e) $Ce_{0.83}Ti_{0.15}Pd_{0.02}O_{2-\delta}$ and (f) $Ce_{0.83}Ti_{0.15}Pt_{0.02}O_{2-\delta}$.

expected that the lattice oxygen utilization takes place resulting in a corresponding reduction of Ce^{4+} to Ce^{3+}. There indeed occurred a reduction in ceria from Ce^{4+} to Ce^{3+} state. However, this reduction was small and is indeed found from the decomposition of the spectra (not presented in the present study). Peaks due to +3 state and distortion of the spectra corresponding to +4 state can be observed only if there occurs a large reduction to +3 state. In most of the spectra after the reaction, Ce seems to be present in +4 state instead of a mixture of +3 and +4 state. Since a large reduction requires large lattice distortion, the reduction was small (10–15%) but some Ce^{3+}–Ce^{4+} transitions indeed occurred.

Figs. 6 and 7 show the XPS of Zr and Ti, respectively in Pd and Pt ion-substituted compounds. Though no reduction can be observed for Zr^{4+} ions, a partial reduction of Ti^{4+} can indeed be observed in case of Ti substituted compounds. Rao et al. have found the presence of only Ce^{4+} and Zr^{4+} in their studies with CeO_2–ZrO_2 compounds [50–52]. We have found that Ce^{4+} and Zr^{4+} are present in the fresh catalyst. After reaction, a partial reduction of Ce^{4+} to Ce^{3+} occurs (Fig. 5(c) and (d)). However, reduction of Zr^{4+} does not take place. We had observed a similar trend in case of the water-gas shift reaction over Pd and Pt metal ion-substituted $Ce_{0.85}Zr_{0.15}O_2$ also [34,53].

The metals in the compounds were present as ions. This was confirmed using XPS. Fig. 8 shows the XPS of Pd3d and Fig. 9 shows the XPS of Pt4f in the various compounds, respectively, before and after reaction. It can be seen from Fig. 8 that Pd was

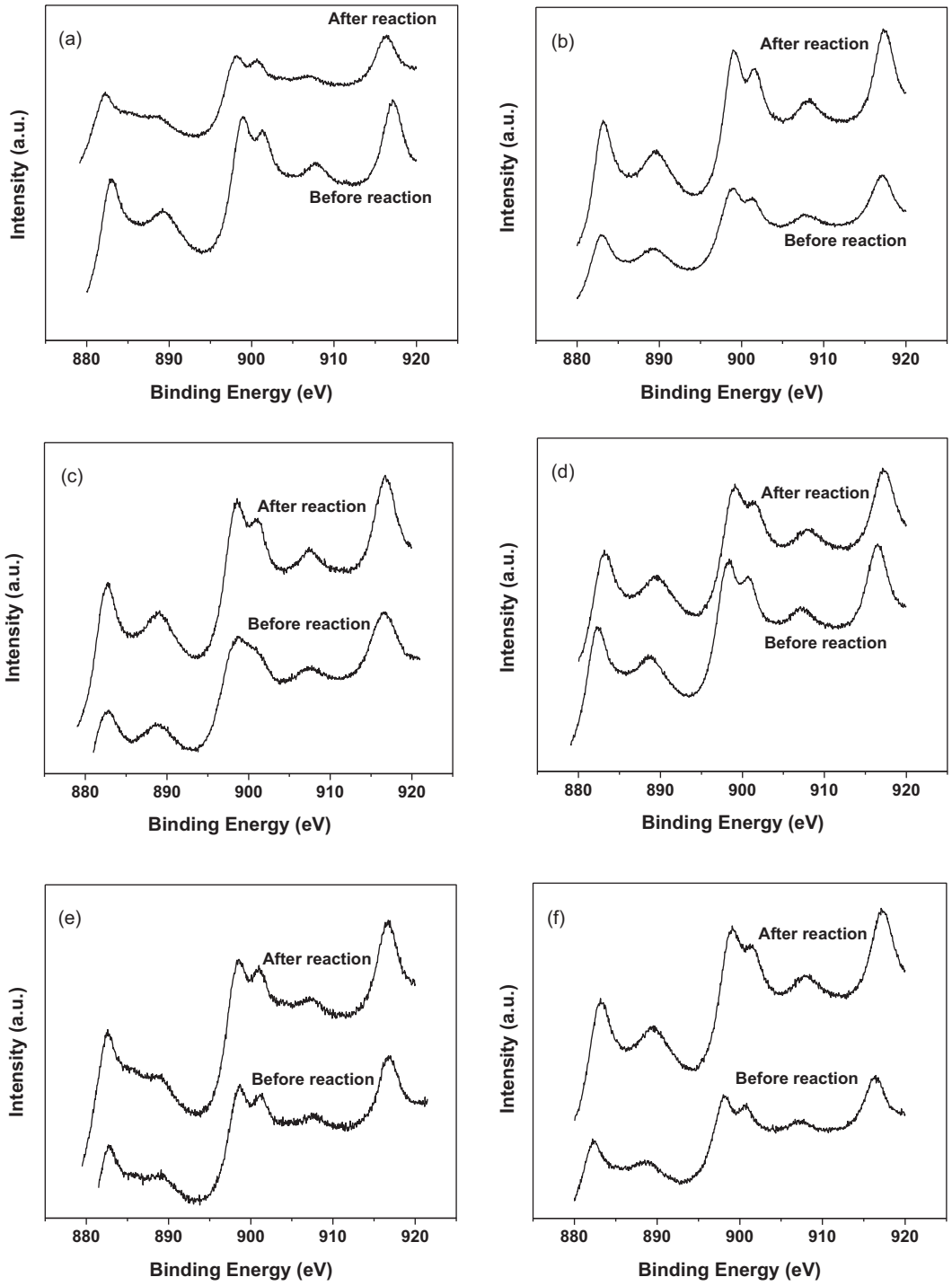

Fig. 5. XPS of Ce3d before and after reaction. (a) $Ce_{0.98}Pd_{0.02}O_{2-\delta}$, (b) $Ce_{0.98}Pt_{0.02}O_{2-\delta}$, (c) $Ce_{0.83}Zr_{0.15}Pd_{0.02}O_{2-\delta}$, (d) $Ce_{0.83}Zr_{0.15}Pt_{0.02}O_{2-\delta}$, (e) $Ce_{0.83}Ti_{0.15}Pd_{0.02}O_{2-\delta}$ and (f) $Ce_{0.83}Ti_{0.15}Pt_{0.02}O_{2-\delta}$.

present in +2 oxidation state in the freshly prepared catalyst. In case of $Ce_{0.83}Zr_{0.15}Pd_{0.02}O_{2-\delta}$, the binding energies of Pd3d and Zr2p are in the same range. Therefore, the spectra were decomposed to give the individual peaks corresponding to Pd3d and Zr2p. The peaks corresponding to Pd3d are marked as solid lines while the peaks corresponding to Zr2p are marked as dashed lines. It can be seen that Pd binding energy for all the compounds was between 237.5 eV and 238 eV. Clearly, Pd was in +2 state. However, after reaction, a small shift in the peaks towards lower binding energies was observed for all the compounds after reaction.

The spectra of Pt4f in all the compounds were decomposed to obtain the individual oxidation states. Fig. 9 shows that Pt was present in ionic form and mixed +2 and +4 oxidation states were observed. The open symbols show the data points obtained from XPS, the thick solid line shows the resultant spectra obtained by decomposing the spectra into individual peaks. The peaks corresponding to +2 state are shown by dashed lines while those corresponding to +4 state are shown by continuous lines. Pt^{2+} and Pt^{4+} binding energies appear at 72 eV and 74 eV, respectively, for the removal of electrons from 4f orbital. The areas under the peaks were used to quantify the amount of Pt in different oxidation states.

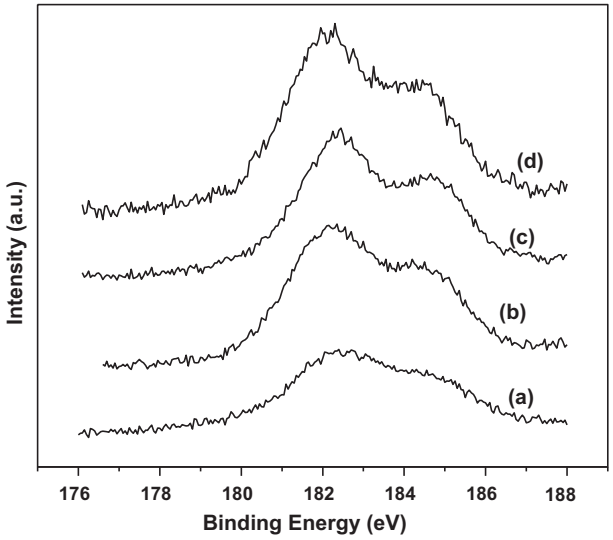

Fig. 6. XPS of Zr3d of (a) $Ce_{0.83}Zr_{0.15}Pd_{0.02}O_{2-\delta}$ before reaction, (b) $Ce_{0.83}Zr_{0.15}Pd_{0.02}O_{2-\delta}$ after reaction, (c) $Ce_{0.83}Zr_{0.15}Pt_{0.02}O_{2-\delta}$ before reaction, (d) $Ce_{0.83}Zr_{0.15}Pt_{0.02}O_{2-\delta}$ after reaction.

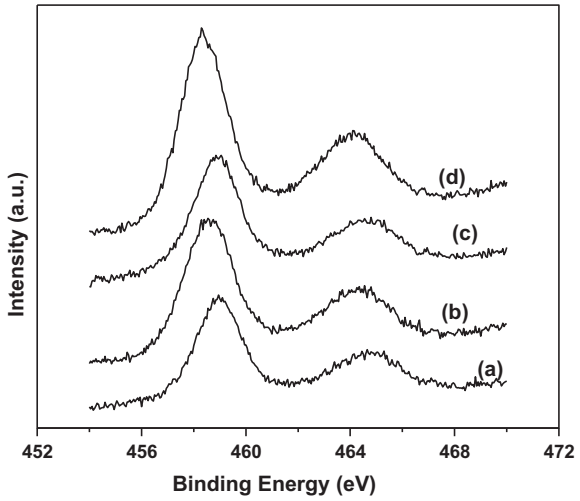

Fig. 7. XPS of Ti2p of (a) $Ce_{0.83}Ti_{0.15}Pd_{0.02}O_{2-\delta}$ before reaction, (b) $Ce_{0.83}Ti_{0.15}Pd_{0.02}O_{2-\delta}$ after reaction, (c) $Ce_{0.83}Ti_{0.15}Pt_{0.02}O_{2-\delta}$ before reaction, (d) $Ce_{0.83}Ti_{0.15}Pt_{0.02}O_{2-\delta}$ after reaction.

Clearly, Pt was present in the ionic state, both before and after reaction. Table 1 gives the percentage of Pt in different oxidation states in different compounds. It can be seen that Pt was mainly in +4 state. However, the oxidation state of Pt was found to change after reaction. In $Ce_{0.98}Pt_{0.02}O_{2-\delta}$, nearly 10% of Pt was present in +2 state which was observed to increase to nearly 20% after reaction. A similar trend was observed in Ti substituted compound also. However,

Table 1
Oxidation states of Pt in the compounds before and after the reaction.

Compound	Pt^{2+}	Pt^{4+}
$Ce_{0.98}Pt_{0.02}O_{2-\delta}$		
Before reaction	9.7%	90.3%
After reaction	19.4%	80.6%
$Ce_{0.83}Zr_{0.15}Pt_{0.02}O_{2-\delta}$		
Before reaction	0.0%	100.0%
After reaction	0.0%	100.0%
$Ce_{0.83}Ti_{0.15}Pt_{0.02}O_{2-\delta}$		
Before reaction	33.8%	66.2%
After reaction	57.8%	42.2%

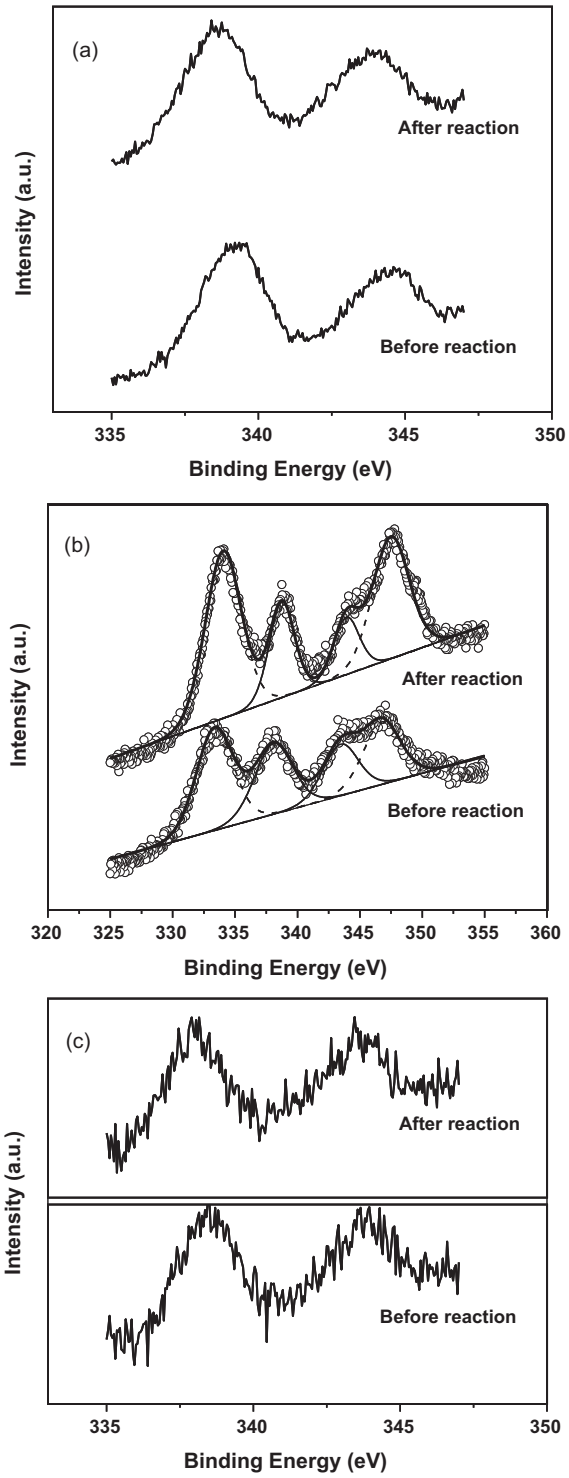

Fig. 8. XPS of Pd3d before and after reaction. (a) $Ce_{0.98}Pd_{0.02}O_{2-\delta}$, (b) $Ce_{0.83}Zr_{0.15}Pd_{0.02}O_{2-\delta}$ and (c) $Ce_{0.83}Ti_{0.15}Pd_{0.02}O_{2-\delta}$.

in Zr substituted compounds, Pt was completely present in +4 state and no considerable reduction was observed after reaction.

The above changes in the oxidation state of the metals can be used for determining the changes in the surface composition and hence the mechanism of the reaction. In all of the cases, it was observed that Ce, which was mainly present in +4 state, underwent a partial reduction to +3 state. This can be due to the highly reducing conditions provided by H_2 in the stream. The following equation

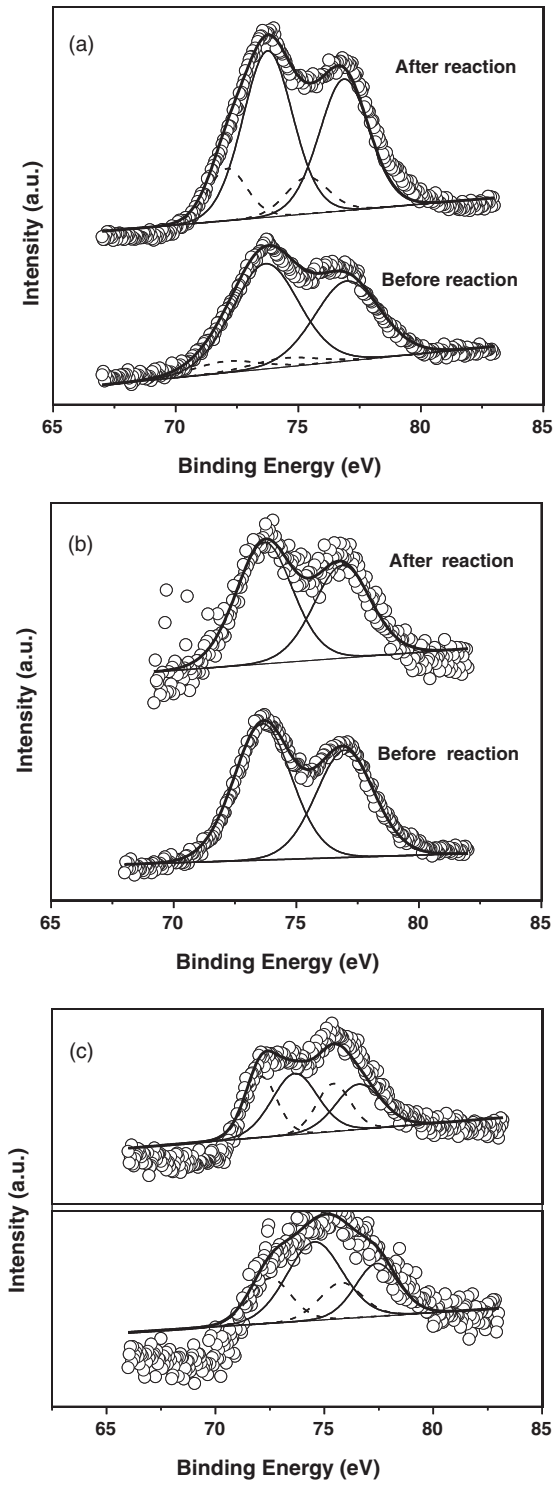

Fig. 9. XPS of Pt4f before and after reaction. (a) $Ce_{0.98}Pt_{0.02}O_{2-\delta}$, (b) $Ce_{0.83}Zr_{0.15}Pt_{0.02}O_{2-\delta}$ and (c) $Ce_{0.83}Ti_{0.15}Pt_{0.02}O_{2-\delta}$.

can be written for this step

$$Ce^{4+}O_2{}^{2-} + \delta H_2 \rightarrow Ce_{2\delta}{}^{3+}Ce_{1-2\delta}{}^{4+}O_{2-\delta}{}^{2-} + \delta H_2O \quad (1)$$

The above equation represents the formation of H_2O utilizing the lattice oxygen, resulting in the formation of Ce^{3+}, which was observed in the XPS. But since metal is also present in ionic form, a reduction of metal ion to lower oxidation states can also take place. This is observed in the XPS of metals, where a partial reduction to lower oxidation states occurs. Because both Ce and the metal ion are reduced and metal in zero state was not observed in the XPS, it can be inferred that electron transfers between Ce and metal take place. Therefore, a metal-support interaction takes place during the reaction and the metal ion gets reduced to the lower oxidation state. The oxidation of the metal ion takes place by a corresponding reduction of support Ce^{4+} ions. These metal-support interactions for the synthesized catalysts for the waste-gas shift reaction have been established previously [34,53]. O_2 from the stream is then consumed in oxidizing the reduced support. This can be represented by the following equation

$$Ce_{2\delta}{}^{3+}Ce_{1-2\delta}{}^{4+}O_{2-\delta}{}^{2-} + \frac{\delta}{2}O_2 \rightarrow Ce^{4+}O_2{}^{2-} \quad (2)$$

However, the involvement of O_2 in the reaction requires further analysis. Thermal treatment of CeO_2 results in the formation of oxide ion vacancies and a part of Ce goes to +3 state [48]. In the freshly prepared catalyst, we have observed Ce to be in only +4 state. However, when a metal ion is substituted in the lattice with an oxidation state other than +4, creation of oxide ion vacancies takes place to maintain the electrostatic neutrality of the compound. The interaction of O_2 with oxide ion vacancies is known and these oxygen deficient sites act as sites for the dissociative adsorption of O_2. According to Colussi et al. [54], the introduction of Pd^{2+} ions in the CeO_2 matrix results in the creation of oxide ion vacancies leading to undercoordinated surface Ce and O atoms and the O atoms near Pd–O sites become more mobile. In this manner, the oxide ion vacancies participate in dissociation of O_2 during the reaction, forming an intermediate oxygen species.

The interaction of H_2 with metal ion is also an important phenomena that occurs during the catalytic cycle. H_2 has been reported to dissociate instantaneously over Pt and Pd metals. In catalysts involving metals, spilling of H atoms to adjacent vacant Pd or Pt sites takes place. Therefore, during the catalytic cycle, it is the multiple site H interaction that results in the formation of the products. However, this phenomenon is different in ionically substituted catalysts like the ones synthesized in this study. It has been shown by the density functional theory calculations that ionic metals can retain more than one H atom on a single site [55]. This results in an increased concentration of H at close vicinity and, therefore, the use of ionic metal is advantageous. Sharma and Hegde [56] have carried out CHC over Pt-impregnated Al_2O_3 catalysts and they have found the activity of these compounds to be lower than that of CeO_2 and TiO_2-based substituted catalysts. We have previously investigated various mechanisms including the conventional Langmuir–Hinshelwood mechanism and the dual site mechanism for oxidation of CO over $Ce_{0.98}Pd_{0.02}O_{2-\delta}$ [57]. It was found that only the dual site mechanism involving the utilization of lattice oxygen satisfactorily explains the experimental observations. Similar observations were also found for noble metal-substituted reducible oxides like TiO_2 [58–59]. The difference in the mechanisms expected over Pd or Pt-impregnated systems and that over the catalysts synthesized in the current study can be understood with the help of Scheme 1.

The dissociation of H_2 over the metal ion is shown in Scheme 1. The H atoms are retained on the same metal site. This is in contrast to the process taking place over metal impregnated systems, where one of the H atoms has to move to the adjacent metal site. The dissociation of O_2 over the oxide ion vacancies takes place, giving the intermediate O species and oxidizing back the reduced catalyst Scheme 1. The interaction of metal and oxide ion vacancy sites result in the formation of the products. In case of metal impregnated catalysts, the two H atoms at two different sites have to interact with adsorbed O_2 or O species, depending upon the type of support involved. Clearly, the two mechanisms are widely different and using metal in ionic form is beneficial for achieving high conversions.

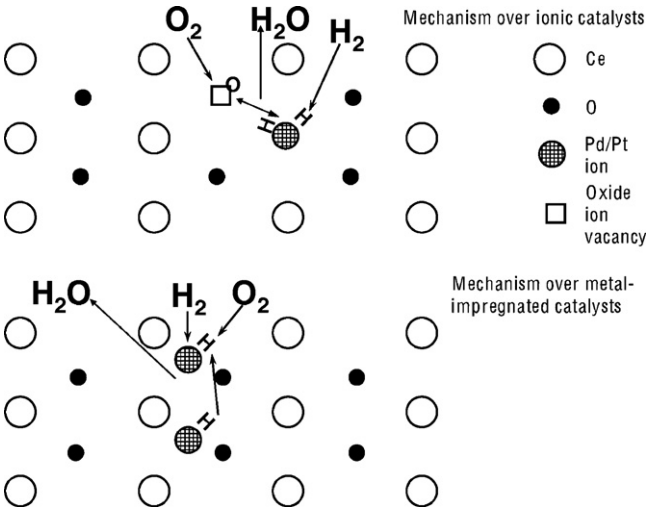

Scheme 1. Surface processes during H_2-combustion over ionic and metal impregnated catalysts.

4. Conclusions

Noble metal ion-substituted catalysts have shown high activity for the catalytic combustion of H_2. The catalysts were found to be CO tolerant and co-oxidation of CO and H_2 took place. The amount of O_2 in the feed was found to have a large effect on the rates of reaction obtained. The reaction was proposed to follow a dual site redox mechanism involving dissociative adsorption of H_2 over the metal ion, dissociative adsorption of O_2 over the oxide ion vacancy and interaction of the intermediate species to release products.

Acknowledgements

PAD would like to thank Bristol-Myers Squibb for the graduate fellowship; GM would like to thank Department of Science and Technology for the Swarnajayanti fellowship; helpful discussions with Prof. M.S. Hegde of SSCU, IISc are gratefully acknowledged.

References

[1] Y. Cengel, M. Boles, Thermodynamics: An Engineering Approach, 6th ed., McGraw-Hill, 2006.
[2] C. Haynes, J. Power Sources 92 (2001) 199–203.
[3] J. Garche, K. Bonhoff, O. Ehret, W. Tillmetz, Fuel Cells 3 (2009) 192–196.
[4] J.L. Silveira, L.A. Gomes, Renew. Sustain. Energy. Rev. 3 (1999) 233–242.
[5] P.C. Buddingh, V. Scaini, L.F. Casey, IEEE Trans. Ind. Appl. 42 (2006) 186–194.
[6] J.P. Vanhanen, P.S. Kauranen, P.D. Lund, Int. J. Hydogen Energy 22 (1997) 707–713.
[7] C.H. Woo, J.B. Benziger, Chem. Eng. Sci. 62 (2007) 957–968.
[8] F. Morfin, J.P. Sabroux, A. Renouprez, Appl. Catal. B: Environ. 47 (2004) 47–58.
[9] M.N. Carcassi, F. Fineschi, Energy 30 (2005) 1439–1451.
[10] D. Gupta, P.G. Deshpande, S.N. Bashyam, Ind. Eng. Chem. Process Des. Dev. 3 (1964) 70–73.
[11] Y.C. Chen, R.W. Bilger, Combust. Flame 131 (2002) 400–435.
[12] Y.C. Chen, R.W. Bilger, Combust. Flame 138 (2004) 155–174.
[13] S. Raimondeau, D. Norton, D.G. Vlachos, R.I. Masel, Proc. Combust. Inst. 29 (2002) 901–907.
[14] D.G. Norton, D.G. Vlachos, Chem. Eng. Sci. 58 (2003) 4871–4882.
[15] D.G. Norton, D.G. Vlachos, Combust. Flame 138 (2004) 97–107.
[16] N.S. Kaisare, G.D. Stefanidis, D.G. Vlachos, Proc. Combust. Inst. 32 (2009) 3027–3034.
[17] N.S. Kaisare, S.R. Deshmukh, D.G. Vlachos, Chem. Eng. Sci. 63 (2008) 1098–1116.
[18] S. Specchia, L.D. Vella, S. Burelli, G. Saracco, V. Specchia, Chem. Phys. Chem. 10 (2009) 783–786.
[19] M. Ladacki, T.J. Houser, R.W. Roberts, J. Catal. 4 (1965) 239–247.
[20] Z. You, I. Balint, K. Aika, Appl. Catal. B: Environ. 53 (2004) 233–244.
[21] P.T. Wierzchowski, L.W. Zatorski, Appl. Catal. B: Environ. 44 (2003) 53–65.
[22] P. Ciambelli, S. Cimino, S. De Rossi, L. Lisi, G. Minelli, P. Porta, G. Russo, Appl. Catal. B: Environ. 29 (2001) 239–250.
[23] L.F. Yang, C.K. Shi, X.E. He, J.X. Cai, Appl. Catal. B: Environ. 28 (2002) 117–125.
[24] K. Persson, L.D. Pfefferle, W. Schwartz, A. Ersson, S.G. Jaras, Appl. Catal. B: Environ. 74 (2007) 242–250.
[25] A.F. Benton, P.H. Emmett, J. Am. Chem. Soc. 48 (1926) 632–640.
[26] R.N. Pease, H.S. Taylor, J. Am. Chem. Soc. 44 (1922) 1637–1647.
[27] A.F. Benton, J.C. Elgin, J. Am. Chem. Soc. 49 (1927) 2426–2438.
[28] A.F. Benton, J.C. Elgin, J. Am. Chem. Soc. 48 (1926) 3027–3046.
[29] L. Petersson, H.M. Dennetun, I. Lundstrom, Surf. Sci. 163 (1985) 273–284.
[30] P.H. Emmett, K.S. Love, J. Phys. Chem. 34 (1930) 41–62.
[31] M.S. Hegde, G. Madras, K.C. Patil, Acc. Chem. Res. 42 (2009) 704–712.
[32] S. Roy, M.S. Hegde, G. Madras, Appl. Energy 86 (2009) 2283–2297.
[33] K.C. Patil, M.S. Hegde, T. Rattan, S.T. Aruna, Chemistry of Nanocrystalline Oxide Materials: Combustion Synthesis, Properties and Applications, World Scientific, Singapore, 2008, pp. 56.
[34] P.A. Deshpande, M.S. Hegde, G. Madras, Appl. Catal. B: Environ. 96 (2010) 83–93.
[35] P. Vidmar, P. Fornasiero, J. Kaspar, G. Gubitosa, M. Graziani, J. Catal. 171 (1997) 160–168.
[36] R. di Monte, J. Kaspar, H. Bradshaw, C. Norman, J. Rare Earths 26 (2008) 136–140.
[37] R. di Monte, J. Kaspar, J. Mater. Chem. 15 (2005) 633–648.
[38] R. di Monte, P. Fornasiero, S. Desinan, J. Kaspar, J.M. Gatica, J.J. Calvino, E. Fonda, Chem. Mater. 16 (2004) 4273–4285.
[39] T. Baidya, G. Dutta, M.S. Hegde, U.V. Waghmare, Dalton Trans. 455 (2009) 455.
[40] E. Aneggi, C. de Leitenburg, G. Dolcetti, A. Trovarelli, Catal. Today 136 (2008) 3–10.
[41] E. Aneggi, C. de Leitenburg, G. Dolcetti, A. Trovarelli, Catal. Today 114 (2006) 40–47.
[42] M. Boaro, V. Modafferi, A. Pappacena, J. Llorca, V. Baglio, F. Frusteri, P. Frontera, A. Troverelli, P.L. Antonucci, J. Power Sources 195 (2010) 649–661.
[43] E. Rocchini, M. Vicario, J. Llorca, C. de Leitenburg, G. Dolcetti, A. Trovarelli, J. Catal. 211 (2002) 407–421.
[44] G. Dutta, U.V. Waghmare, T. Baidya, M.S. Hegde, K.R. Priolkar, P.R. Sarode, Catal. Lett. 108 (2006) 165.
[45] C.R. Henry, C. Chapon, C. Duriz, Z. Phys. D Atom Mol. Cl. 19 (1991) 347.
[46] B.A. Sexton, A.E. Hughes, Surf. Sci. 140 (1984) 227–248.
[47] V.P. Zhdanov, Surf. Sci. 169 (1986) 1–13.
[48] A. Trovarelli (Ed.), Catalysis by Ceria and Related Materials, Imperial College Press, London, 2002.
[49] A. Trovarelli, M. Boaro, E. Rocchini, C. de Leitenburg, G. Dolcetti, J. Alloys Compd. 323–324 (2001) 584–591.
[50] G. Ranga Rao, J. Kaspar, R.D. Monte, S. Meriani, M. Graziani, Catal. Lett. 24 (1994) 107–112.
[51] G. Ranga Rao, P. Fornasiero, R.D. Monte, J. Kaspar, G. Vlaic, G. Balducci, S. Meriani, G. Gubitosa, A. Cremona, M. Graziani, J. Catal. 162 (1996) 1–9.
[52] P. Fornasiero, G. Ranga Rao, J. Kaspar, F.L. Erario, M. Graziani, J. Catal. 175 (1998) 269–279.
[53] P.A. Deshpande, G. Madras, AIChE J. 56 (2010) 2662–2676.
[54] S. Colussi, A. Gayen, M.F. Camellone, M. Boaro, J. Llorca, S. Fabris, A. Trovarelli, Angew. Chemie. Int. Ed. 48 (2009) 8481–8484.
[55] G. Dutta, U.V. Waghmare, T. Baidya, M.S. Hegde, Chem. Mater. 19 (2007) 6430–6436.
[56] S. Sharma, M.S. Hegde, Chem. Phys. Chem. 10 (2009) 637–640.
[57] S. Roy, A. Marimuthu, M.S. Hegde, G. Madras, Appl. Catal. B: Environ. 71 (2007) 23–31.
[58] S. Roy, A. Marimuthu, M.S. Hegde, G. Madras, Appl. Catal. B: Environ. 73 (2007) 300–310.
[59] S. Roy, M.S. Hegde, S. Sharma, N.P. Lalla, A. Marimuthu, G. Madras, Appl. Catal. B: Environ. 84 (2007) 341–350.